



7N-28
193710
P27

TECHNICAL NOTE

D-287

EFFECT OF TRANSVERSE ACOUSTIC OSCILLATIONS ON THE VAPORIZATION OF A LIQUID-FUEL DROPLET

By Paul R. Wieber and William R. Mickelsen

Lewis Research Center
Cleveland, Ohio

NATIONAL AERONAUTICS AND SPACE ADMINISTRATION

WASHINGTON

May 1960

(NASA-TN-D-287) EFFECT OF TRANSVERSE
ACOUSTIC OSCILLATIONS ON THE VAPORIZATION OF
A LIQUID-FUEL DROPLET (NASA. Lewis
Research Center) 27 p

N89-70932

Unclas
00/28 0198710

NATIONAL AERONAUTICS AND SPACE ADMINISTRATION

TECHNICAL NOTE D-287

EFFECT OF TRANSVERSE ACOUSTIC OSCILLATIONS ON THE
VAPORIZATION OF A LIQUID-FUEL DROPLET

By Paul R. Wieber and William R. Mickelsen

SUMMARY

A theoretical analysis of the effect of a standing transverse acoustic field on the vaporization of a liquid n-octane droplet was made. Three differential equations were developed to express the drop acceleration in the axial and transverse directions and the rate of change in radius of the drop with time, defined as the vaporization rate. The equations were solved on an analog computer for a range of gas conditions, drop diameters from 10 to 500 microns, axial gas velocities from 0 to 800 feet per second, and acoustic fields with frequencies of 200, 1000, and 4000 cycles per second with root-mean-square transverse gas velocities from 0 to 400 feet per second. Histories of the drop velocities, displacements, radius, and rate of change of radius with time were obtained.

Results of this analysis show that in an acoustic field a drop acquires an oscillating transverse velocity and a fluctuating vaporization rate. The time required to vaporize 97 percent of the drop mass was reduced as acoustic-field frequency and amplitude were increased. The increase in vaporization rate was suggested as a possible cause of the increased combustion efficiency noted under unstable combustion conditions for an initially inefficient combustor.

A parameter $\Delta E/E$, the energy release ratio, was defined as the ratio of the magnitude of periodic fluctuations in the vaporization rate over the mean vaporization rate. The ratio $\Delta E/E$ expresses the tendency of drop vaporization to support a gas wave and was found to be dependent on an approximate Reynolds number over the range $0 < Re_E < 500$. Characteristic Reynolds number Re_E was based on the root-mean-square difference between the maximum transverse gas velocity and the maximum transverse drop velocity achieved near the time when the vaporization-rate fluctuation was at its peak. This dependency suggests that, for a given dissipation in a vaporization-controlled process, large drops would more easily amplify disturbances than small drops.

INTRODUCTION

One common form of unstable combustion that may occur in both rocket and jet engine combustors is characterized by high-frequency pressure and particle-velocity waves. These waves have been identified with geometric resonant acoustic modes of oscillation. One effect of such an acoustic field can be a marked rise in the combustion efficiency of an initially inefficient system, as noted in reference 1 for a resonating rocket engine. This increase suggests that, if vaporization is the limiting step in the combustion process as noted in reference 2, there may be an interaction between vaporization rate and combustion instability.

Many studies of the vaporization and motion of droplets under simulated stable combustion conditions have been made (e.g., refs. 3 to 7). Under extremely severe resonance in the longitudinal mode the pulses become shock-fronted. The effect of such shock waves on droplets has been studied in references 8 to 10. Reference 11 presents an experimental study of the combustion of droplets mechanically suspended in a cool vibrating airfield. However, the vaporization of a single drop has not been investigated in an acoustic field where all the heat transferred to the drop is supplied by the hot bulk-gas flow rather than by the burning mantle surrounding the drop.

The effect of gas-velocity oscillations on the vaporization of a hydrocarbon fuel droplet has been analyzed theoretically at the NASA Lewis Research Center for a range of combustor conditions. The model chosen for this study consisted of a drop injected into a steady axial gas flow on which was superimposed a standing transverse sinusoidal oscillation. The drop was assumed to be injected on the axis of the combustor so that pressure effects could be neglected. The fuel was designated as normal octane, and the gas as air. Five initial drop diameters were chosen: 10, 30, 100, 250, and 500 microns. The gas temperatures were 700°, 1000°, and 1300° R; pressures were 0.3, 1.0, and 2.0 atmospheres; and relative axial velocities between the gas and drop were 0, 200, 500, and 800 feet per second. The acoustic field was defined for frequencies of 200, 1000, and 4000 cycles per second with the root-mean-square acoustic particle velocity of the gas ranging from 0 to 400 feet per second. The combinations of these conditions selected for study represented the worst, average, and most favorable vaporization conditions that exist in jet combustors, plus two combinations for the largest drops.

The initial gas conditions used in this study were restricted in range, since some of the equations introduced in the derivation were experimentally valid only for conditions found in jet engines. However, the drop size range was expanded to include the larger drops that might

be found in rocket engines, and the results were nondimensionalized for generality.

Equations describing the vaporization of a drop and its acceleration in the axial and transverse directions were developed. The equations were solved on an analog computer, and drop histories were obtained. Vaporization trends are presented, and a discussion is included which offers suggestions for a mechanism for developing and sustaining high-frequency combustion instability.

SYMBOLS

A_{cs}	projected area of drop, sq ft
C_D	coefficient of drag
\bar{c}	root-mean-square velocity of gas molecules evaluated at surface temperature of drop, cm/sec
D	molecular mass diffusivity of vapor, sq ft/sec
$\Delta E/E$	$\frac{(\dot{dr}/dt)_{\max} - (\dot{dr}/dt)_{\min}}{\frac{1}{2}[(\dot{dr}/dt)_{\max} + (\dot{dr}/dt)_{\min}]}$
F	force, lb
g	gravitational constant = 32.17 ft/sec ² or 980 cm/sec ²
H_V	latent heat of vaporization of liquid, Btu/lb
k	thermal conductivity, Btu/(sq ft)(sec)(°F)/ft
l	mean free path of gas molecules, cm
M	molecular weight, lb/lb-mole
m	mass of drop, slugs
P	gas pressure, lb/sq ft
Re	Reynolds number, $\frac{2r\rho_{g,m}\Delta V}{\mu_{g,m}}$

Re_E	characteristic Reynolds number, $\frac{2r\rho_{g,m}(\sqrt{v^2} - \sqrt{v_d^2})}{\mu_{g,m}}$
r	radius of drop, ft
Sc	Schmidt number, $\mu_{g,m}/D\rho_{v,m}$
T	temperature, °R
t	time, sec
U	velocity of gas in axial direction, ft/sec
ΔV	total velocity difference, ft/sec
v	velocity of gas in transverse direction, ft/sec
$\sqrt{v^2}$	root-mean-square transverse gas velocity, ft/sec
$\sqrt{v_d^2}$	root-mean-square value of maximum transverse drop velocity, ft/sec
μ	viscosity, lb/(ft)(sec)
ρ	density, lb/cu ft

Subscripts:

d	drop
g	gas
l	liquid
m	indicates that quantity is evaluated at a mean temperature
max	instantaneous maximum
min	instantaneous minimum
o	initial condition of quantity
t	total
v	vapor
x	axial direction downstream from injection
y	transverse direction away from line of injection

THEORETICAL ANALYSIS

The droplet under consideration is injected on the axis of a long cylindrical combustor, as shown in figure 1. The combustor is experiencing an acoustic field of the first standing transverse mode with a pressure profile, as shown in figure 2. There are no pressure fluctuations at the injection point and, as long as deflections from the axis are small, pressure fluctuations are negligible as shown in reference 12. Therefore, the model fits any case where pressure does not affect vaporization, as in references 13 and 14. The drop is subjected to a constant axial stream velocity U , which tends to drive it down the combustor in the x-direction, and a sinusoidal transverse gas velocity v , which may be at any fraction of its maximum amplitude at the instant of injection and tends to drive the drop back and forth across the combustor in the y-direction. Shock waves are excluded from this model, as is drop shattering. The drop experiences no heating period, an assumption that becomes erroneous for drops of low volatility as explored quantitatively in reference 6.

The two gas velocities produce forces on the droplet, so that it acquires the component drop velocities U_d and v_d in the x- and y-directions, respectively. The vector resultant of the velocity differences between gas and drop is then

$$\Delta V = \left[(U - U_d)^2 + (v - v_d)^2 \right]^{0.5} \quad (1)$$

The aerodynamic pressure force on a drop is given by the drag equation

$$F_d = \rho_g A_{cs} \frac{\Delta V^2}{2} C_D \quad (2)$$

In reference 3, an empirical expression for the drag coefficient for experiments is derived. It is

$$C_D = 27/Re^{0.84} \quad (3)$$

where the Reynolds number is based on the average film temperature of the drop. This drag-coefficient expression is used in equation (2), and the experimental conditions used in reference 3 apply in this analysis. An assumption that the drop does not change the properties, composition, and velocity of the gas eliminates any effects of the drop oscillating in its own wake when the relative axial velocity between the gas and drop is zero. However, the boundary layer must readjust itself at each change of direction, and the use of the drag-coefficient equation was extrapolated for some conditions beyond the Reynolds number range investigated in reference 3. This makes the use of equation (3) in this model questionable, but no drag-coefficient values have been obtained under all the conditions investigated herein.

When equations (1) and (3) are substituted into (2), the total force on the drop becomes

$$F_{d,t} = 23.7 r^{1.16} \frac{\rho_g}{\rho_{g,m}} \mu_{g,m}^{0.84} \left[(U - U_d)^2 + (v - v_d)^2 \right]^{0.58} \quad (4)$$

The resultant force on the drop $F_{d,t}$ has the same direction as the resultant velocity at any instant in time. The geometries of the relative velocities and forces on the drop in the resultant and x directions give

$$\frac{F_{d,x}}{F_{d,t}} = \frac{U - U_d}{\left[(U - U_d)^2 + (v - v_d)^2 \right]^{0.5}} \quad (5)$$

From the momentum equation, the force on the drop in the x-direction may also be expressed as

$$F_{d,x} = \frac{4}{3} \frac{\rho_l \pi r^3}{g} \frac{d(U_d)}{dt} \quad (6)$$

Substituting equations (6) and (4) into (5) gives, on simplification,

$$\frac{d(U_d)}{dt} = 182 \frac{1}{\rho_l} \frac{1}{r^{1.84}} \frac{\rho_g}{\rho_{g,m}} \mu_{g,m}^{0.84} \left[(U - U_d)^2 + (v - v_d)^2 \right]^{0.08} (U - U_d) \quad (7)$$

for the acceleration of the drop in the x-direction.

In like manner, consideration of the y-components of the force and relative-velocity geometries leads to

$$\frac{d(v_d)}{dt} = 182 \frac{1}{\rho_l} \frac{1}{r^{1.84}} \frac{\rho_g}{\rho_{g,m}} \mu_{g,m}^{0.84} \left[(U - U_d)^2 + (v - v_d)^2 \right]^{0.08} (v - v_d) \quad (8)$$

the acceleration of the drop in the y-direction.

In reference 15 the following expression for the rate of change of mass of a drop with time was developed:

$$\frac{dm}{dt} = \frac{k_{g,m}(T_g - T_l)}{H_V} 4\pi r \left[1 + 1.29 \times 10^6 \left(\text{Re Sc} \frac{gl}{c^2} \right)^{0.6} \left(\frac{k_{g,m}}{k_{v,m}} \right)^{0.5} \right] \quad (9)$$

Applying the ideal gas law and equation (1) gives

$$\text{Re Sc} = \frac{2r}{D} \frac{T_m}{T_g} \frac{M_g}{M_l} \left[(U - U_d)^2 + (v - v_d)^2 \right]^{0.5} \quad (10)$$

For air,

$$\frac{gl}{c^2} = \frac{2.56 \times 10^{-12}}{P_t} \text{ atm}$$

If equation (10) and the relation between dm and dr are substituted in equation (9), the result is the following expression for the rate of change of radius with time, which is defined as the vaporization rate of the drop:

$$\frac{dr}{dt} = \frac{k_{g,m}(T_g - T_l)}{\rho_l r H_V} \left(1 + 1.29 \times 10^6 \left\{ \frac{2r T_m M_g}{P_t D T_g M_l} \left[(U - U_d)^2 + (v - v_d)^2 \right]^{0.5} \right. \right. \\ \left. \left. 2.56 \times 10^{-12} \right\}^{0.6} \left(\frac{k_{g,m}}{k_{v,m}} \right)^{0.5} \right) \quad (11)$$

Equations (7), (8), and (11) were solved simultaneously to give drop histories.

Examination of these three equations indicates that a cross-coupling would be expected between the acceleration equations, since $U - U_d$ and $v - v_d$ are included in both equations. The vaporization rate decreases as the drop accelerates toward the constant stream velocity, but the $(v - v_d)^2$ quantity should produce a rectified fluctuation in the vaporization rate as long as v_d lags behind v . Although pressure effects are excluded from this study, it is noted that the transverse drop displacement causes the drop to oscillate through a small pressure gradient. Depending on the time phase of the displacement with the gas-velocity and vaporization-rate fluctuations, the varying pressure could cause a further increase or decrease in the vaporization-fluctuation amplitude.

PROCEDURE

Acoustic particle root-mean-square velocities from 0 to 400 feet per second were investigated, since reference 12 shows that the transverse particle velocity may be comparable to the axial gas velocity in magnitude. The maximum particle velocity corresponds to a ratio of root-mean-square sound pressure to ambient pressure of about 0.45 (ref. 12, fig. 2). For simplicity it was assumed that the drop injection velocity was zero and that all relative axial velocity was produced by the gas. The fuel was designated as n-octane, and the gas as air. Physical properties were found from data and equations in references 4, 6, 15, and 16.

The equations were solved by an analog computer. A block diagram of the circuit is shown in figure 3. Because of the large number of loops in the circuit, reproducibility errors due to random circuit noise varied from 1/2 to 2 percent for the shortest to the longest time required for the computer to complete each solution. Noise is interpreted by the computer as increased relative velocity between the gas and drop, and thus tends to shorten vaporization time. A large precision error resulted from the necessity of approximating the raising of the function $[r^2(\Delta V)^2]$ to the 0.08 and 0.3 exponents. Instead of a smooth power curve of input against output, three straight lines were used for each exponent. This gave a precision error of from 1 to 5 percent on the function only. Noise in the exponent circuits gave a maximum error of 2 percent on the function, but only at the end of the problem. The maximum overall error is believed to be 3 to 4 percent, and this was reduced slightly by 1/2 to 1 percent by adjusting the data with an empirical noise-correction factor.

As the radius decreased, scaling factors increased outputs of parts of the circuit to intolerable levels, so that the problem was automatically stopped when the radius reached 0.3 its original value, corresponding to 97.3 percent of the mass vaporized. The output of the analog gave plots of drop radius, displacement in the y-direction, velocity in the x- and y-directions, vaporization rate, and transverse gas velocity against time, and radius against axial displacement.

As a test case, the vaporization of a 30-micron-diameter drop was run under the conditions of figure 10 in reference 4. The analog solution gave agreement within 1 percent of the vaporization time obtained from the plot of drop diameter against vaporization time (fig. 10, ref. 4).

RESULTS AND DISCUSSION

Drop Histories

The drop histories are illustrated by figure 4. The time required for the drop to vaporize to 0.3, its initial radius, is referred to as the vaporization time.

Radius. - The plot of drop radius with time is illustrated in figure 4(f). As the acoustic particle velocity and frequency increase, the negative slope of the radius curve becomes greater. If an axial gas velocity is present, the radius curve shows a small initial dip. Some combinations of drop size and acoustic-field intensity give the curve of radius against time a slight ripple as the vaporization rate fluctuates.

Displacements. - The maximum displacement of the drop in the transverse direction increases as the transverse gas velocity increases and as the frequency of oscillation and inertia of the drop decrease. Generally, the maximum displacement was below 10 percent of the combustor radius, so that the assumption of no significant pressure effects appears valid. If the transverse gas velocity is less than its maximum amplitude at the time of injection, the drop is initially displaced from its injection point and oscillates thereafter around a new mean position, as shown in figure 4(c). This process may contribute to the mixing in the combustor. The axial displacement of the drop is roughly proportional to the axial gas velocity.

Axial velocity. - The curve in figure 4(b) is typical for the variation of axial drop velocity with time. Upon impact the drop quickly accelerates asymptotically toward the axial fluid stream velocity. As the transverse-gas-velocity amplitude increases, cross-coupling effects cause the axial acceleration of the drop to increase also. For some conditions the U_d curve shows a slight ripple as $(v - v_d)^2$ fluctuates, as shown in figure 5(a).

Transverse velocity. - The transverse drop velocity v_d plotted against time produces three types of profiles, as illustrated in figure 6. With the first type (fig. 6(a)), v_d closely follows the transverse gas velocity. Type 2 (fig. 6(b)) shows a v_d profile whose peak amplitude increases slightly near the end of the drop history. The third type shows an immediate increase in maximum v_d amplitude to a relatively larger value, after which maximum amplitude remains constant, as shown in figure 6(c) and to a lesser extent in figure 4(d).

The peaks of the individual v_d curves for the profiles in figures 6(b) and (c) are flattened, indicating a lag between the gas and the drop. The cross-coupling between the equations also appears for low values of v_d as shown by figure 5(b), where the initially large v_d amplitudes diminish as $U - U_d$ decreases.

Vaporization rate. - The plot of dr/dt , the vaporization rate, against time also shows three different profiles, as illustrated in figure 6. Figure 6(a) shows dr/dt as a smooth curve that rises at an accelerating rate as the drop radius decreases. The second type of dr/dt profile is a series of fluctuations whose maximum amplitude decreases as the drop vaporizes, as shown in figure 6(b). Figures 6(c) and 4(a) illustrate the type-3 dr/dt trace, which is also a series of humps. However, the peak amplitude of each fluctuation passes through a maximum as the drop history progresses.

The individual fluctuations that occur in types 2 and 3 dr/dt profiles have an irregular shape that changes as the drop vaporizes. The low points of each fluctuation are defined by the vaporization rate for that instantaneous drop radius when the gas and drop have no velocity differences, assuming that the drop boundary layer is adjusting to the gas conditions instantly.

The v_d and dr/dt curves in each of figures 6(a) to (c) occur in pairs. A decrease in the maximum amplitude of the dr/dt curves indicates that $v - v_d$ is decreasing through changes in either the amplitude of v_d or the lag of v_d behind v , or both. Comparison of each set of curves gives a good qualitative picture of the interaction between the oscillating transverse gas and drop.

Very small drops (10-micron diam.) at any condition and medium small drops (30 microns) at low acoustic-field frequencies produce the type-1 profiles in figure 6(a). The low inertia of these drops enables them to follow the oscillating gas almost perfectly. The second set of profiles, shown in figure 6(b), occurs for combination of low aerodynamic forces and initially high drop inertia such as medium (100-micron diam.) and large (250- and 500-micron diam.) drops with lower gas velocities and frequencies, and medium small drops with higher frequencies. Type 3 of v_d and dr/dt profiles (fig. 6(c)) tends to occur for high-inertia medium and large drops in strong acoustic fields. The increase in peak-to-peak v_d amplitude occurs immediately after injection; this increase is large - as much as 300 feet per second for one situation.

The reduction in vaporization time by the acoustic field, which is discussed in the next section, varies according to the type of v_d and dr/dt profiles that occur. There is little or no decrease in vaporization time for systems producing type-1 profiles. Type-2 systems show

vaporization-time reductions from small to large amounts, and only type-3 profiles give the greatest reductions due to the acoustic field.

Effect of Acoustic Field on Vaporization Time

The reduction in vaporization time is shown by τ , the ratio of the time to vaporize to $0.3r_0$ with an acoustic field present to the vaporization time with the field absent. For constant oscillation frequencies, τ is plotted against root-mean-square acoustic particle velocity in figures 7 and 8.

Figure 7(a) shows the effect of the acoustic field for the 10-micron-diameter drop. The most severe acoustic field gives a maximum of only 5 percent reduction in τ . The vaporization is relatively insensitive to amplitude of the transverse gas velocity because the drop tracks the gas almost perfectly. Frequency has a little more effect on τ because of the extremely short vaporization time that limits the number of cycles the drop is subjected to before vaporization.

The 30-micron drop has a long enough life and greater inertia, so that the acoustic field can affect it as shown in figure 7(b). As the drop begins to lag behind the gas, increasing transverse gas amplitude and frequency decrease τ more severely. Figure 7(b) also illustrates that the same reduction of vaporization time by the acoustic field occurs with or without an axial gas velocity, as shown by the solid line for $U = 0$ and the broken line for $U = 500$ feet per second. The curves are quite close, and this same relatively minor effect occurs for all drop sizes.

The reduction in τ for the 100-micron drop is shown in figure 7(c). Vaporization time becomes greatly reduced by an increase in particle velocity of the oscillations. Most of the amplitude effect occurs at root-mean-square particle velocities greater than 25 feet per second. Increasing frequency also produces a large reduction in τ , but the spread between the curves at 1000 and 4000 cycles per second indicates that frequency effects are less important at high frequencies. The high frequencies reduce the drop maximum transverse velocity toward zero, or else produce a lag that keeps a large velocity difference between drop and gas. A comparison of drop histories verifies that there is a large difference in the maximum v_d amplitudes between frequencies of 200 to 1000 cycles per second, but maximum v_d values for 1000 and 4000 cycles per second are more nearly alike. This indicates that the large inertia forces restrict the drop from following both frequencies to about the same degree.

Figure 8 shows the vaporization-time ratio for the 250- and 500-micron-diameter drops at the same gas temperature and pressure. The trend of less sensitivity to frequency continues for these two large drops as the three frequency curves are converging. Wave amplitude has a very large effect on these drops; it reduces the vaporization time to one-sixth its original value for the 500-micron drop in the most severe acoustic field. Large reductions in τ occur for small root-mean-square gas-velocity increases beyond 25 feet per second. After a $\sqrt{v^2}$ value of 250 feet per second, increases in amplitude have little effect on vaporization time.

The lessening of vaporization time for all cases may be an explanation for the higher combustion efficiency observed in unstable combustors that are initially inefficient. The large drops have the longest vaporization times under normal combustion conditions, and it is possible for them to enter the nozzle area without complete vaporization. These large drops were the most severely affected by the acoustic field. Perhaps the shorter vaporization time would allow a larger percentage of the fuel to vaporize and burn in the chamber, which would improve the combustion efficiency.

Effect of Acoustic Field on Instantaneous Vaporization Rate

The fluctuations of the vaporization rate dr/dt with time were investigated further. Since a small change in radius is approximately proportional to a small change in mass, these waves roughly represent the variation in the loss of mass of the drop as vapor that may then be burned to add energy to the gas perturbation. If the peak and low points of each dr/dt fluctuation are defined as $(dr/dt)_{\max}$ and $(dr/dt)_{\min}$, respectively, then a parameter $\Delta E/E$, the energy release ratio, can be defined as

$$\frac{\Delta E}{E} = \frac{(dr/dt)_{\max} - (dr/dt)_{\min}}{\frac{1}{2} [(dr/dt)_{\max} + (dr/dt)_{\min}]}$$

which is illustrated in figure 4(a).

The denominator of this parameter represents the arithmetic-mean level of energy addition to the gas, and the numerator expresses the fluctuation of energy addition around that mean level. The maximum value of $\Delta E/E$ is 2.0.

For each drop history five or six measurements of $\Delta E/E$ were taken at the peaks of dr/dt fluctuations. The peak amplitude of the v_d cycle nearest to the sampling point was recorded with the drop radius

for each measurement. The radius was substituted into a Reynolds number expression defined as Re_F , where the velocity difference used was specified as the $\sqrt{v^2}$ value for that drop history minus the root-mean-square value of the peak v_d near the point of measurement. This Reynolds number is approximate, since it is not based on the exact velocity difference at the dr/dt sampling point.

Curves of $\Delta E/E$ against Re_F and their envelopes of data points are shown in figure 9 for drop sizes of 30-, 100-, 250-, and 500-micron diameters. The 10-micron drop for all frequencies and the 30-micron drop for the frequency of 200 cycles per second showed no detectable dr/dt fluctuations; Re_F was always below 5.0 for the 10-micron drop and was below 15.0 for the 30-micron drop at 200 cycles per second.

To get an approximate idea of the time phase between the transverse gas velocity and the energy addition, an instantaneous value of the transverse gas velocity v was taken at each $\Delta E/E$ sample and was divided by the maximum transverse gas velocity occurring in that drop history. This gave the v at the instant of maximum energy addition in terms of the fraction of maximum transverse gas velocity attainable. The percentage of runs for each fraction is listed in figure 9. This measurement is very crude, especially for the higher frequencies.

Figure 9 shows that at low values of Re_F a small increase in Re_F gives a very large increase in $\Delta E/E$. Then, after Re_F equals 500, a very large increase in Re_F is required to give an appreciable $\Delta E/E$ increase. Any curve of figure 9 includes data for all the frequencies and root-mean-square gas velocities investigated for one initial drop size. The table in figure 9 of v/v_{max} against percent of data samples shows that, in a majority of the samples, the maximum energy addition occurs when the gas velocity is over half of its maximum attainable values.

The energy required to support a gas perturbation must be preferentially added to the gas at a time when it will support the pulse rather than cancel it (ref. 17).

It may be assumed that the normalized increment in energy release rate per cycle $\Delta E/E$ is related to the ease of initiation of resonance and to the equilibrium amplitude for a fixed dissipation. On this basis any combustion process for which a perturbation can produce a change in rate of energy release (vaporization, mixing, atomization, gas-phase kinetics) can drive the system into resonance.

For the vaporization process discussed in this paper, figure 9 indicates that for small velocity differences $\Delta E/E$ is very sensitive to

drop size; whereas for large velocity differences the effect of drop size on $\Delta E/E$ is relatively small. This suggests that in a combustion system that is vaporization-controlled, a collection of large drops would be more conducive to the growth of small disturbances in velocity than a collection of small drops. It also suggests that the large drops should lead to somewhat higher resonance amplitudes than the small drops for a given dissipation. These suggestions, of course, do not consider the effects of pressure and of actual drop size distributions that require further study.

It is instructive, nevertheless, to test these ideas with the experimental data listed in table I of reference 18. When only the two spray nozzles are considered, the trend of amplitude of resonance with drop size is the reverse of that just mentioned and correlates approximately with the intensity of combustion E . The data for the impingement atomization injectors are anomalous until the effects of disturbances are considered. If impingement is impaired or prevented by a velocity perturbation, the resultant drops will be very large compared with those resulting from impingement, and this in turn will lead to a large value of $\Delta E/E$ per cycle and should produce the larger amplitudes observed. Jet breakup or variations in mixing would produce a similar effect. Although the data are meager and not altogether conclusive, it can be tentatively concluded that both the values of E and $\Delta E/E$ are factors in the stability of a combustion system. Further study is required to determine their relative importance and to establish the role of the dissipation phenomena in determining equilibrium resonance amplitudes.

CONCLUSIONS

The calculation of the history of the liquid-fuel droplet in a standing transverse acoustic field gave the following trends.

The reduction in the time to vaporize 97.3 percent of the drop mass due to the transverse acoustic field becomes greater with increasing drop diameter, transverse-gas-velocity amplitude, and frequency of oscillations. Large drops on the order of 500 microns may experience a reduction to almost one-sixth of the vaporization time with no acoustic field. It was suggested that this overall increase in vaporization rate may explain in part the high combustion efficiency observed in resonating combustors that are initially inefficient.

A parameter $\Delta E/E$, the energy release ratio, was assumed to show the tendency of drop vaporization to support a gas perturbation. This was related to a characteristic Reynolds number Re_E based on the difference between maximum gas and drop velocities. The ratio $\Delta E/E$ was

found to increase rapidly with increase of Re_E until Re_E was around 500. Thereafter $\Delta E/E$ made only moderate increases. The behavior of $\Delta E/E$ with respect to drop size and relative transverse velocity suggests that large drops would more easily amplify disturbances in a vaporization-controlled process than small drops.

Lewis Research Center

National Aeronautics and Space Administration
Cleveland, Ohio, March 11, 1960

REFERENCES

1. Heidmann, M. F., and Auble, C. M.: Injection Principles from Combustion Studies in a 200-Pound-Thrust Rocket Engine Using Liquid Oxygen and Heptane. NACA RM E55C22, 1955.
2. Priem, Richard J.: Propellant Vaporization as a Criterion for Rocket-Engine Design; Calculations Using Various Log-Probability Distributions of Heptane Drops. NACA TN 4098, 1957.
3. Ingebo, Robert D.: Drag Coefficients for Droplets and Solid Spheres in Clouds Accelerating in Airstreams. NACA TN 3762, 1956.
4. Ingebo, Robert D.: Vaporization Rates and Heat-Transfer Coefficients for Pure Liquid Drops. NACA TN 2368, 1951.
5. Ingebo, Robert D.: Vaporization Rates and Drag Coefficients for Isooctane Sprays in Turbulent Air Streams. NACA TN 3265, 1954.
6. Priem, Richard Jerome: Vaporization of Fuel Drops Including the Heating-Up Period. Ph.D. Thesis, Univ. Wis., 1955.
7. Probert, R. P.: The Influence of Spray Particle Size and Distribution in the Combustion of Oil Droplets. Phil. Mag., ser. 7, vol. 37, no. 265, Feb. 1946, pp. 94-105.
8. Hanson, A. R., Domich, E. G., and Adams, H. S.: An Experimental Investigation of Impact and Shock-Wave Break-Up of Liquid Drops. Rep. 125, Rosemount Aero. Lab., Univ. Minn., Nov. 15, 1955.
9. Priem, Richard J.: Breakup of Water Drops and Sprays with a Shock Wave. Jet Prop., vol. 27, no. 10, Oct. 1957, pp. 1084-1087; 1093.
10. Engel, Olive G.: Fragmentation of Waterdrops in the Zone Behind an Air Shock. Jour Res. Nat. Bur. Standards, vol. 60, no. 3, Mar. 1958, pp. 245-280.

11. Kumagai, Seiichiro, and Isoda, Hiroshi: Combustion of Fuel Droplets in a Vibrating Air Field. Fifth Symposium (International) on Combustion, Reinhold Pub. Corp., 1955, pp. 129-132.
12. Mickelsen, William R.: Effect of Standing Transverse Acoustic Oscillations on Fuel-Oxidant Mixing in Cylindrical Combustion Chambers. NACA TN 3983, 1957.
13. Spalding, D. B.: A One-Dimensional Theory of Liquid-Fuel Rocket Combustion. Rep. 20,175, British ARC, May 19, 1958.
14. Mayer, E.: Vaporization Rate Limited Combustion in Bipropellant Rocket Chambers. ARS Jour., vol. 29, no. 7, July 1959, pp. 505-513.
15. Ingebo, Robert D.: Study of Pressure Effects on Vaporization Rate of Drops in Gas Streams. NACA TN 2850, 1953.
16. Keenan, Joseph H., and Kaye, Joseph: Thermodynamic Properties of Air. John Wiley & Sons, Inc., 1945.
17. Rayleigh: The Theory of Sound. Vols. 1-2. Dover Pub., 1945.
18. Feiler, Charles E.: Effect of Fuel Drop Size and Injector Configuration on Screaming in a 200-Pound-Thrust Rocket Engine Using Liquid Oxygen and Heptane. NACA RM E58A20a, 1958.

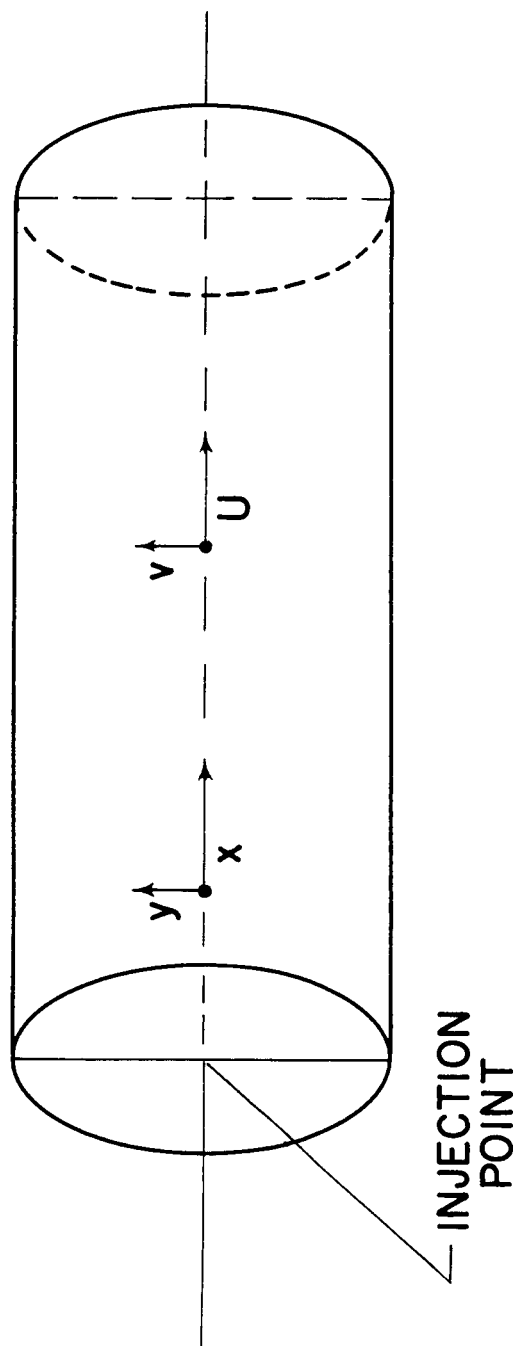


Figure 1. - Combustor coordinate system.

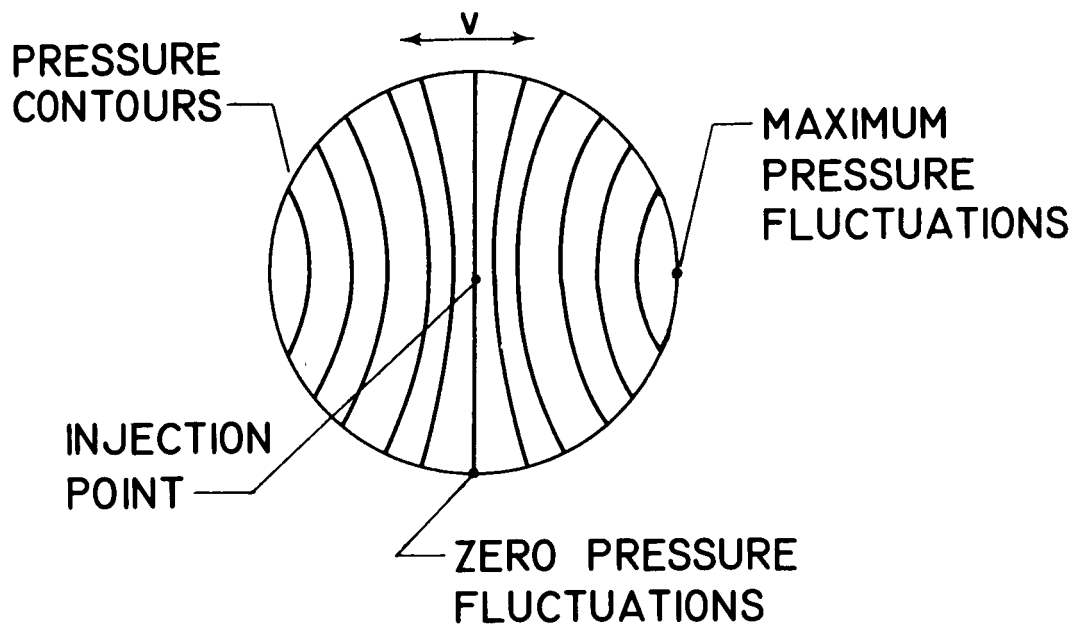
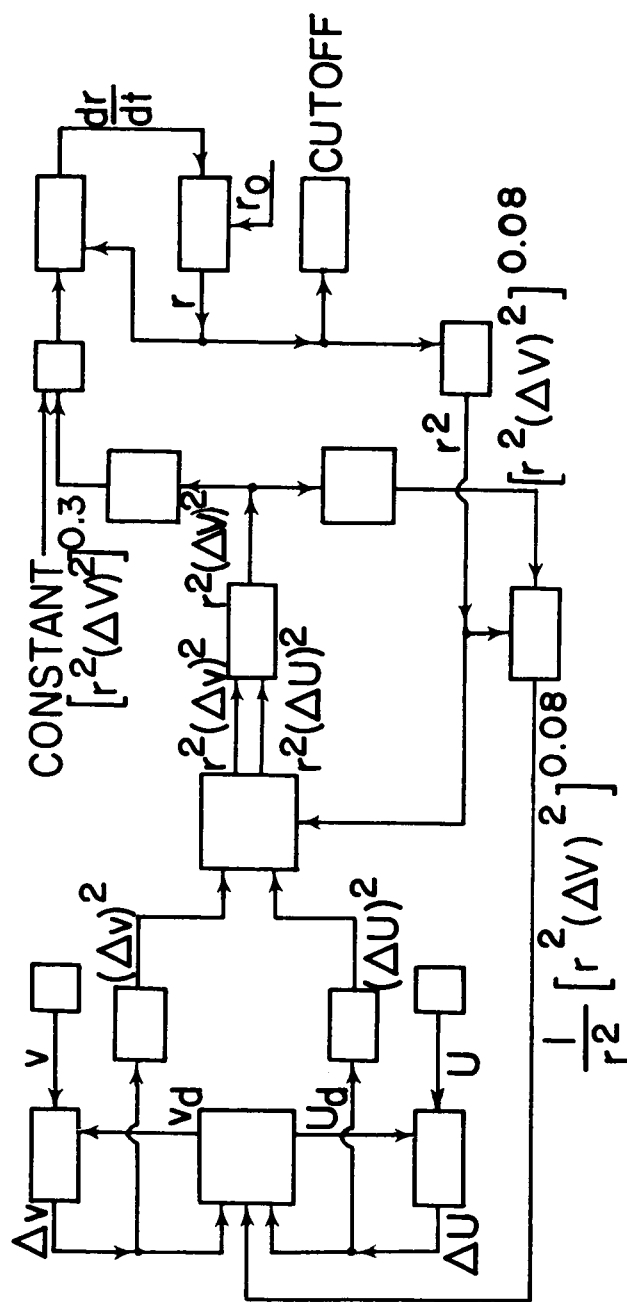


Figure 2. - Pressure contours in combustor experiencing first standing transverse mode.



$$\begin{aligned}
 U - U_d &= \Delta U \\
 v - v_d &= \Delta v \\
 (U - U_d)^2 + (v - v_d)^2 &= (\Delta V)^2 \\
 \text{CONSTANTS NOT INCLUDED}
 \end{aligned}$$

Figure 3. - Block diagram of analog circuit.

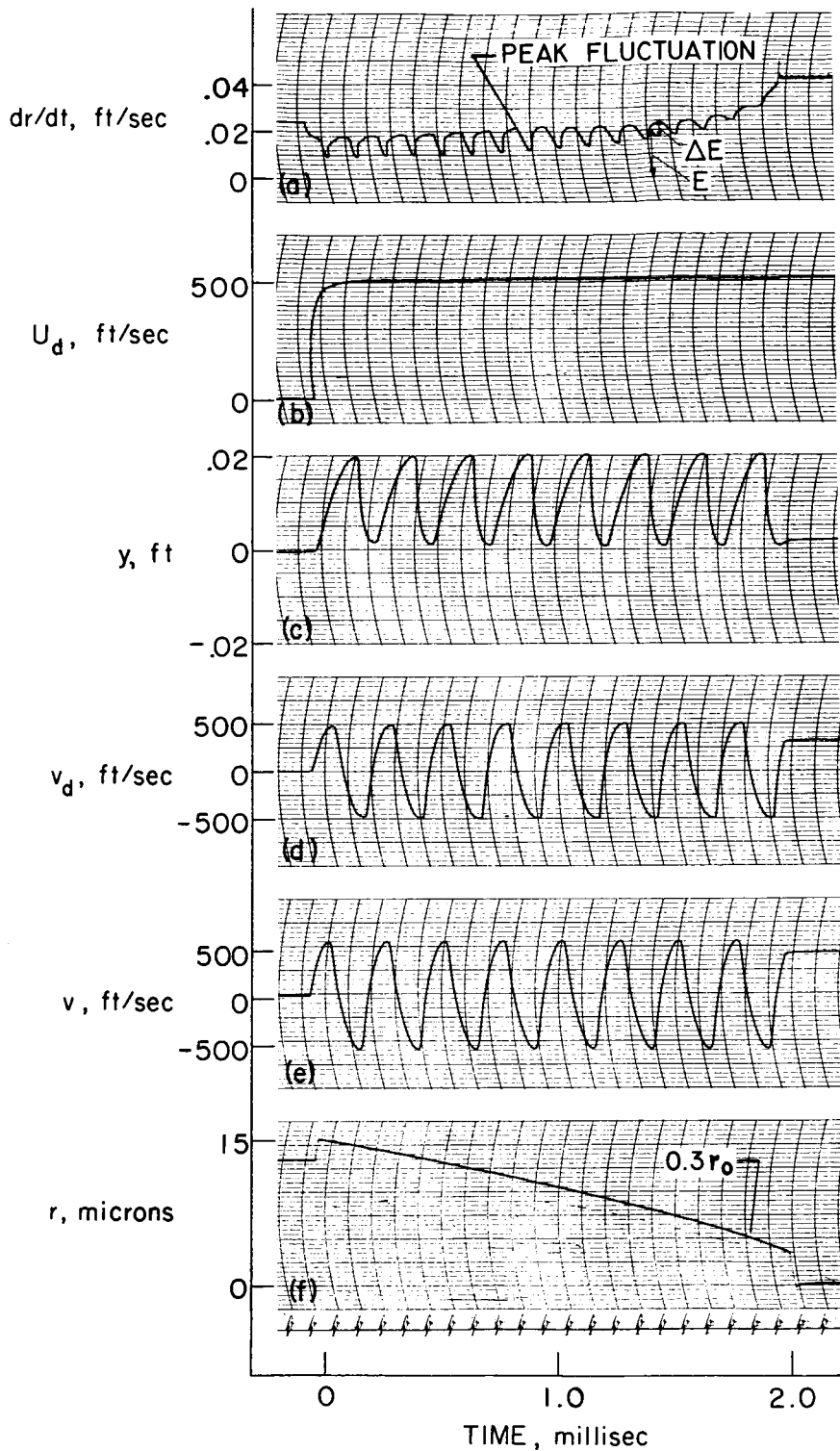
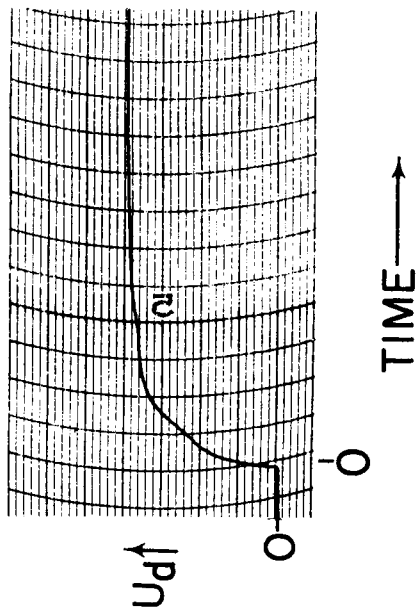
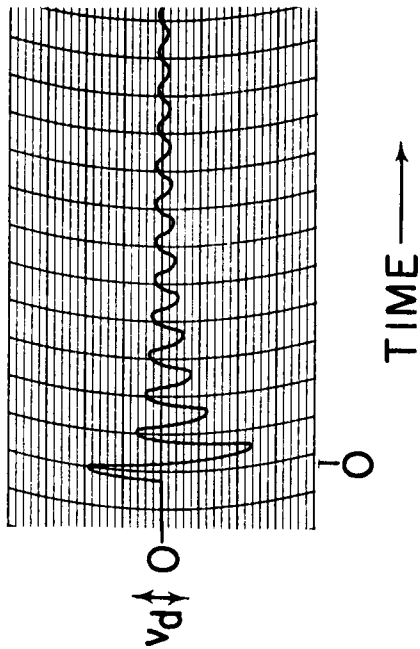


Figure 4. - Typical drop-history data. $2r_0$, 30μ ; $\sqrt{v^2}$, 400 feet per second; f , 4000 cycles per second; T , $1000^\circ R$; P , 1 atmosphere; U , 500 feet per second.

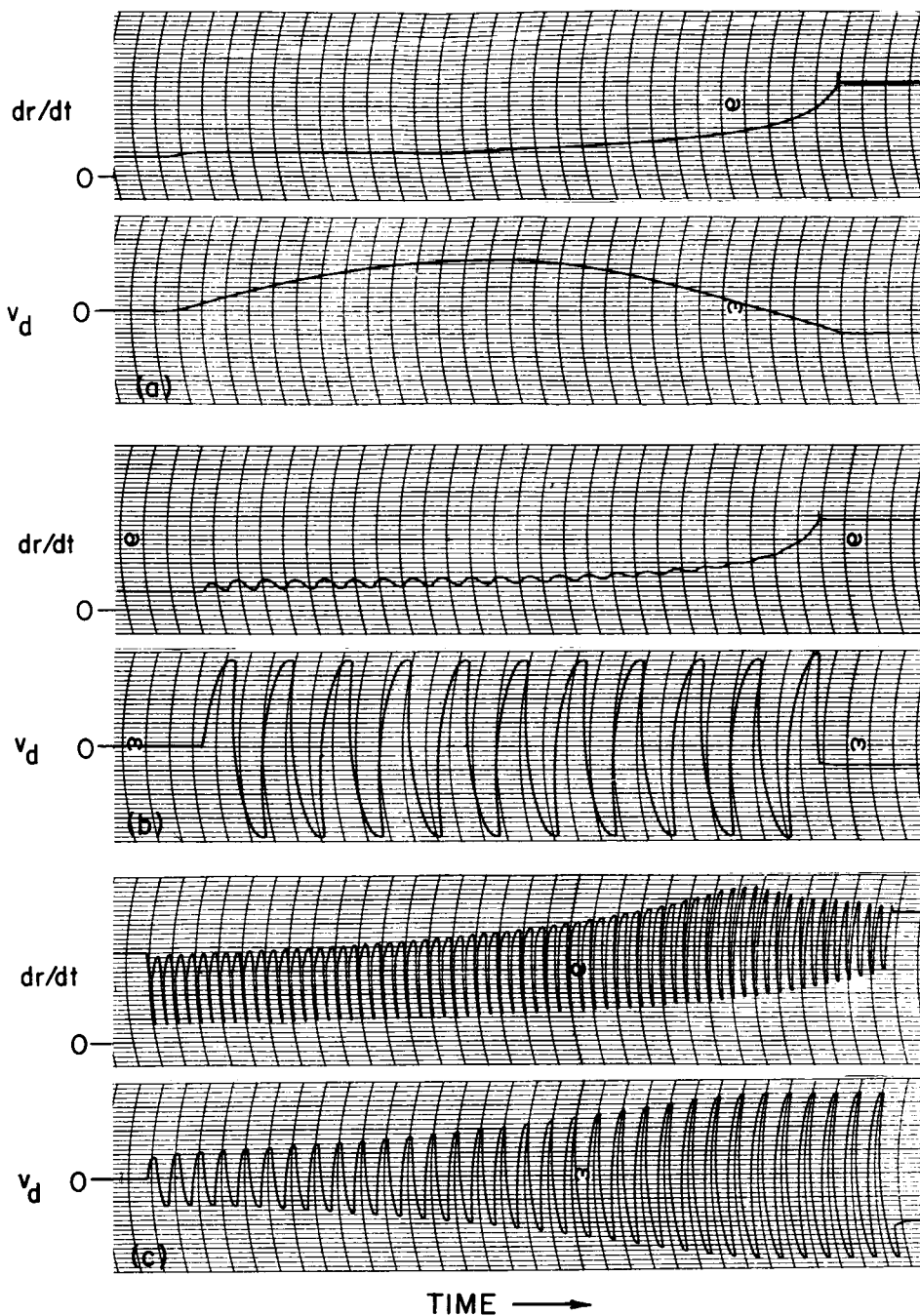


(a) $2r_o$, 250 microns; U , 200 feet per second; $\sqrt{V^2}$, 100 feet per second; f , 200 cycles per second.



(b) $2r_o$, 250 microns; U , 200 feet per second; $\sqrt{V^2}$, 25 feet per second; f , 1000 cycles per second.

Figure 5. - Plots of axial drop velocity and transverse drop velocity against time, illustrating cross-coupling effects.

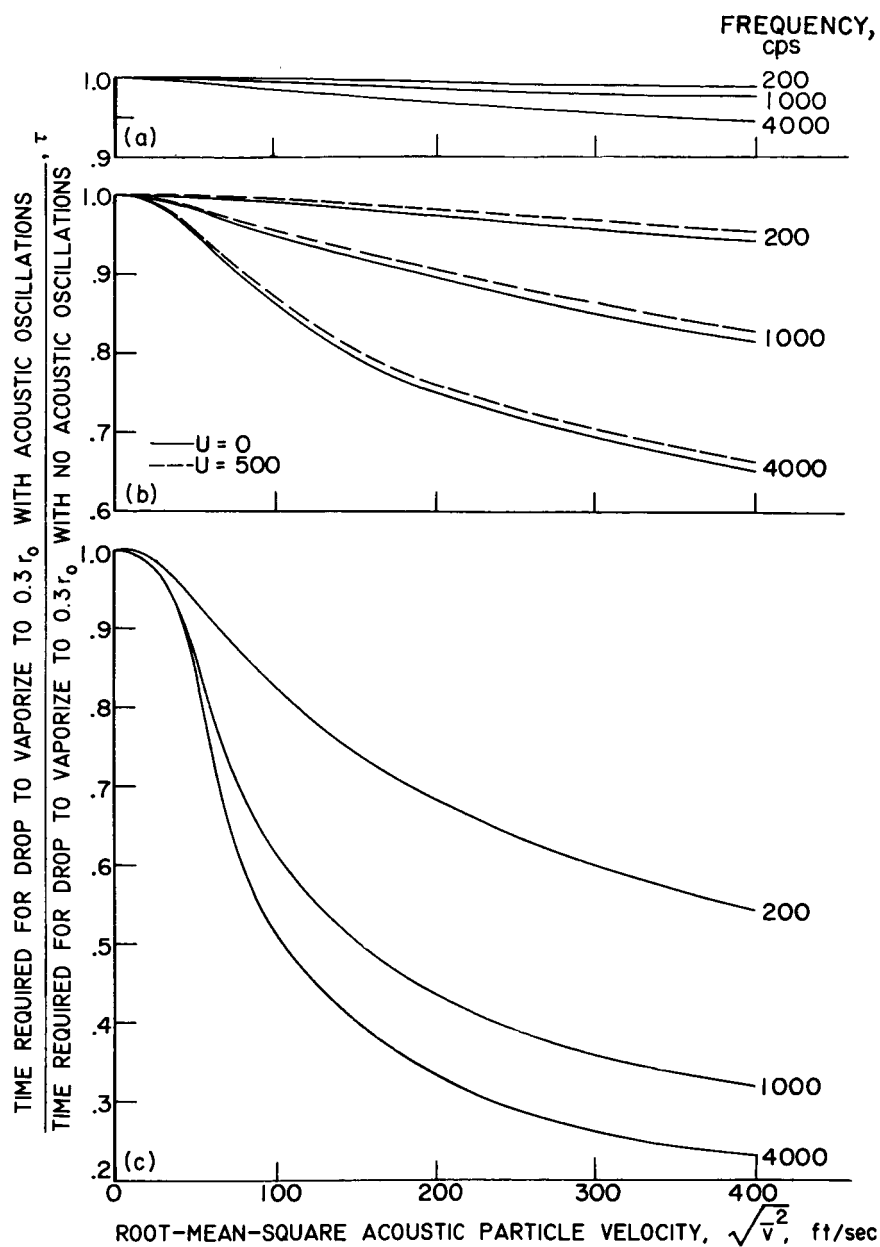


(a) Type 1. $2r_0$, 30 microns; $\sqrt{v^2}$, 400 feet per second; f , 200 cycles per second.

(b) Type 2. $2r_0$, 30 microns; $\sqrt{v^2}$, 100 feet per second, f , 4000 cycles per second.

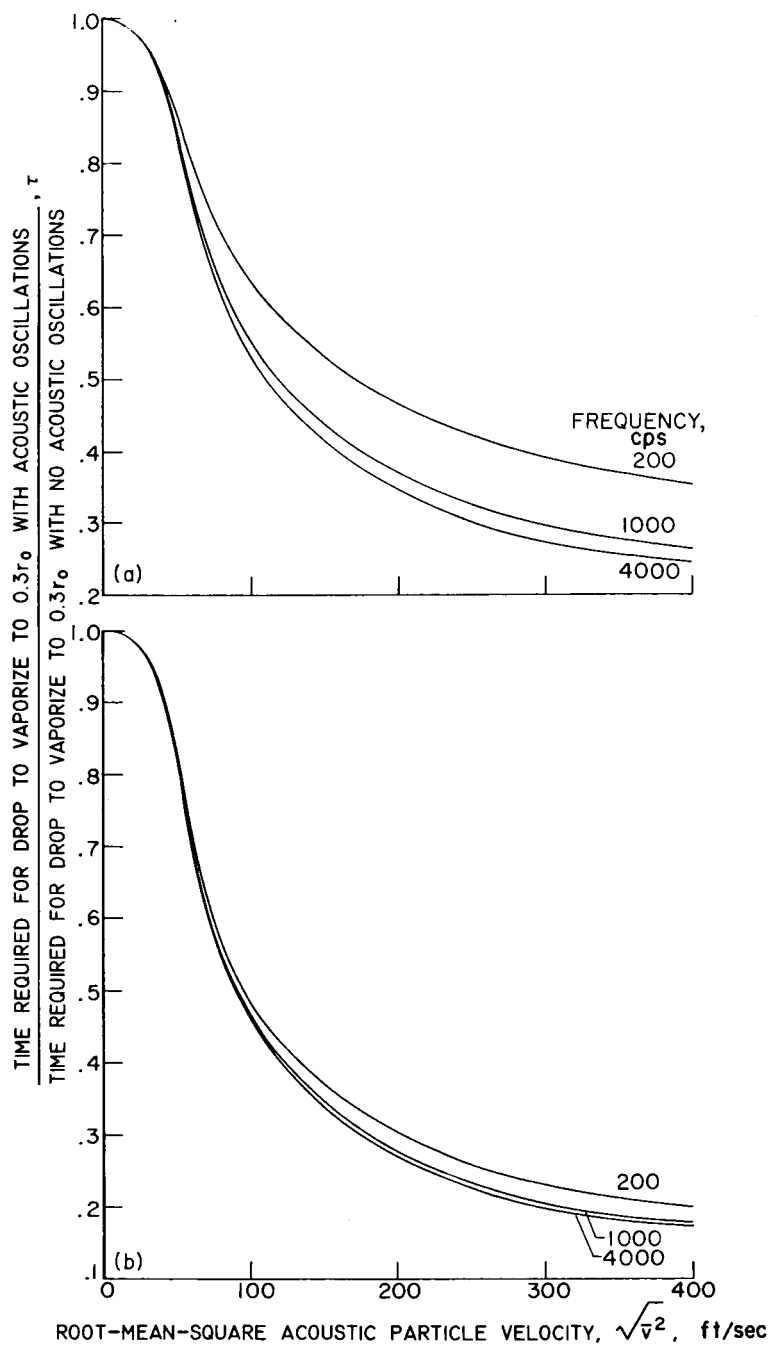
(c) Type 3. $2r_0$, 250 microns; $\sqrt{v^2}$, 250 feet per second; f , 1000 cycles per second.

Figure 6. - Plots of three sets of v_d and dr/dt profiles against time; $U = 0$.



- (a) $2r_0$, 10μ ; T_g , 1300°R ; P , 0.3 atmosphere; U , 0.
- (b) $2r_0$, 30μ ; T_g , 1000°R ; P , 1.0 atmosphere; U , 0 and 500 feet per second.
- (c) $2r_0$, 100μ ; T_g , 700°R ; P , 2.0 atmospheres; U , 0.

Figure 7. - Variation of τ , the ratio of time required to vaporize drop to $0.3r_0$ with acoustic field to time required with no acoustic field, with root-mean-square acoustic particle velocity.



(a) $2r_0$, 250 μ ; T_g , 1300° R; P, 2.0 atmospheres; U, 0.

(b) $2r_0$, 500 μ ; T_g , 1300 R; P, 2.0 atmospheres; U, 0.

Figure 8. - Variation of τ , the ratio of time required to vaporize drop to $0.3r_0$ with acoustic field to time required with no acoustic field, with root-mean-square acoustic particle velocity.

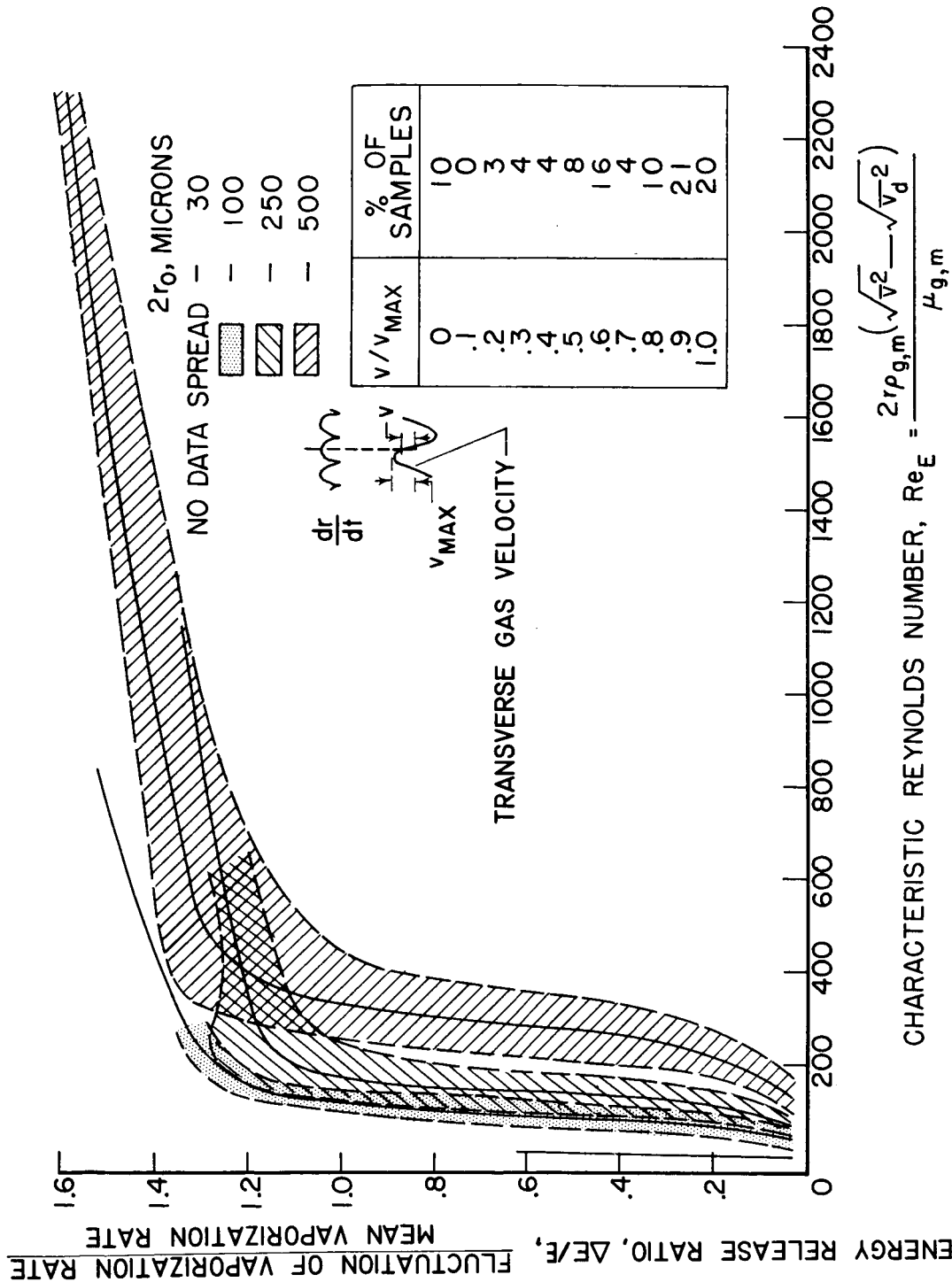


Figure 9. - Variation of energy release fluctuations over mean-energy release level with approximate Reynolds number expression for vaporizing drops.